COMMUNICATION

Co-presence of PtNi Nanowires and Ionic Liquid in Carbon Mesopores Enhances Electrocatalytic Oxygen Reduction Activity

Received 00th January 20xx,
Accepted 00th January 20xx

DOI: 10.1039/x0xx00000x

Yuta Kato,[a] Masaru Kato,[a,b]* Shun Saito,[a] Yu Zhuang,[a] Yoshimi Iguchi,[a] Jun Sato,[c] Tasuku Komanoya,[c] Kentaro Soma,[d] Koshiro Suzuki,[a] Ichizo Yagi[a,b]*

The electrocatalytic activity of PtNi nanowires is enhanced by the co-presence of ionic liquid in carbon mesopores. Three-dimensional transmission electron microscopy tomography and surface-enhanced infrared absorption spectroscopy confirm the co-presence of PtNi nanowires and ionic liquid inside carbon mesopores even under electrochemical conditions.

Pt alloy nanostructured electrocatalysts supported on carbon have been widely used for electrochemical devices such as polymer electrolyte fuel cells (PEFCs)[1-3] and water electrolyzers.[4-6] In the nanostructured electrocatalysts, Pt and Pt alloy nanowires (NWs) are highly active for the oxygen reduction reaction (ORR), which is known to be catalyzed at the cathode in PEFCs and metal-air batteries, and their mass activity (MA) can reach 13.6 A $(mg_{Pt})^{-1}$ at 0.9 V vs. RHE using a rotating disk electrode (RDE).[7] The MA of Pt-based electrocatalysts for the ORR is also known to be severely reduced in the membrane-electrode assembly (MEA) for practical PEFCs: the highest MA in an MEA to date is 1.77 A $(mg_{Pt})^{-1}$,[8] which is an order of magnitude lower than the highest MA in the RDE.[2,3,7] This drastic MA loss in the MEA is mainly due to the limitation of mass transport in the catalyst layer, where Pt-based nanocatalysts are covered with ionomer films such as Nafion, which provide proton transport pathways but also block oxygen transport.[1-3] Thus, the suppression of ionomer poisoning remains a challenge for Pt alloy nanostructured electrocatalysts.

The use of small amounts of hydrophobic ionic liquids (ILs) with Pt-based electrocatalysts, which is known as the solid catalyst with ionic liquid layer (SCILL) concept, improves O_2 solubility[9,10] and/or suppress the formation of non-reactive Pt-O(H) species at the catalyst surface,[11,12] resulting in high ORR activity for Pt-based electrocatalysts.[9-15] The SCILL approach can be applied especially to nanostructured Pt alloy catalysts with open framework[15] and nanopore structures,[9,10] where capillary force pulls ILs. Similarly, ILs can also be encapsulated in mesoporous carbon supports.[16] It is expected that both of Pt-based catalysts and ILs can be kept inside carbon mesopores, leading to maximizing the catalytic activity of Pt-based catalysts without poisoning by ionomers.[1,3,17-20] The encapsulation of Pt-based NWs in carbon mesopores can provide not only the ionomer-free Pt surface but also higher proton conductivity along the NW, compared with nanoparticles, even in carbon mesopores, predicted by model studies.[21] However, the encapsulation of NWs in carbon mesopores has not been reported: it was believed that NWs (typically ≤5 nm in diameter)[7,22-30] could not be placed inside the pores of mesoporous carbon supports.[1]

Herein, we report the effect of IL-modification on the electrocatalytic activity of PtNi NWs supported on a mesoporous carbon for the ORR in acidic media. As an IL, 1-butyl-3-methylimidazolium hexafluorophosphate ([BMIM][PF_6]) was mainly used in this work.[11,12,14] To confirm the co-presence of NWs and the IL in carbon mesopores, 3D electron tomography and *in situ* surface-enhanced infrared absorption (SEIRA) spectroscopy of the electrocatalyst were performed.

PtNi NWs were prepared from the precursor mixture of [Pt(acac)$_2$] (acac = acetylacetonate), [Ni(acac)$_2$], glucose, [$Mo(CO)_6$], and cetyltrimethylammonium chloride in oleylamine at 433 K under the air for 2 h (See the Supporting Information, SI).[28] The atomic ratio of Pt:Ni for PtNi NWs was determined to be about 95:5 by ICP-MS. The XRD pattern of PtNi NWs resembles that of Pt/C (**Fig. S1**) and PtNi NWs previously reported.[28] The NWs were immobilized on two carbon blacks commercially available: one is Vulcan XC-72R with a BET specific surface area of 223 $m^2\ g^{-1}$ and the other is a mesoporous carbon of CNovel MJ(4)010-00 with 1240 $m^2\ g^{-1}$ and a pore diameter of 10 nm. PtNi NWs supported on Vulcan XC-72R and CNovel MJ(4)010-00 are referred to in this paper as PtNi NW/C and PtNi NW/mesoC, respectively.

Scanning transmission electron microscopy (STEM) images of PtNi NW/C and PtNi NW/mesoC show the homogeneous

[a] *Graduate School of Environmental Science, Hokkaido University, N10W5, Kita-ku, Sapporo 060-0810, Japan*
[b] *Faculty of Environmental Earth Science, Hokkaido University, N10W5, Kita-ku, Sapporo 060-0810, Japan. Emails: masaru.kato@ees.hokudai.ac.jp (MK); iyagi@ees.hokudai.ac.jp (IY)*
[c] *R&D Center, Business Creation Sector, Mitsui Mining and Smelting Co., Ltd., 1333-2, Haraichi, Ageo 362-0021, Japan*
[d] *Materials Analysis & Exploration Center, Mitsui Mining and Smelting Co., Ltd., 1333-2, Haraichi, Ageo 362-0021, Japan*
Electronic Supplementary Information available: [details of any supplementary information available should be included here]. See DOI: 10.1039/x0xx00000x

immobilization of NWs on both supports (**Fig. S2** in the Electronic Supplementary Information, **ESI**). The diameter of the NWs is 1.7±0.1 nm, which is smaller than the diameter of the mesopores of mesoC. Three-dimensional high-angle annular dark field (HAADF)-STEM tomography of PtNi NW/mesoC visualized that NWs are not only located on the surface but also inside mesopores (**Fig. 1** and a video in the **SI**). Since isolated NWs are simply mixed with mesoC to prepare PtNi NW/mesoC, the insertion of NWs into mesopores is thermodynamically favorable: possibly entropy-driven insertion involving removal of surfactants from the surface of NWs.[31]

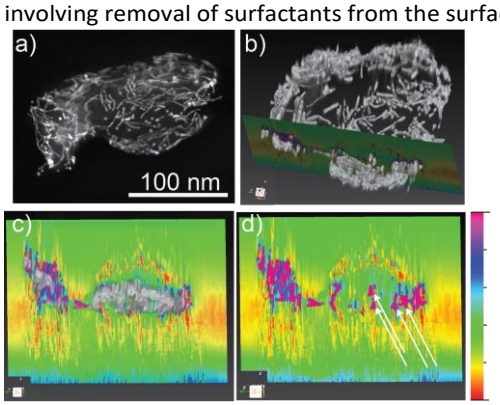

Fig. 1 (a) HAADF-STEM and (b) 3D reconstruction images achieved by HAADF-STEM tomography for PtNi NW/mesoC. (c,d) Cross-sectional images are sliced images at the plane shown in (b) with and without 3D reconstructed volume image of NWs, respectively. The magenta regions show particularly high intensity voxels in HAADF-STEM images, which are correlated to high electron density distribution in the PtNi NW/mesoC, corresponding to PtNi NWs. The arrows indicate the NWs placed inside mesopores. A video on the tomography is also available in the SI.

Cyclic voltammograms (CVs) of PtNi NW/mesoC and PtNi NW/C were recorded in a 0.1 M $HClO_4$ aqueous solution under Ar (**Fig. S3**). Both catalysts show cathodic and anodic waves associated with the adsorption and desorption of the underpotentially deposited hydrogen (Hupd) on Pt(111) ranging between 0.05 and 0.30 V vs. RHE overlapping the Hupd on Pt(100) at about 0.3 V vs. RHE.[32] The difference in current densities in this potential range between PtNi NW/mesoC and PtNi NW/C suggests that the electrolyte accessibility to the Pt surface of NWs is suppressed by ionomers for PtNi NW/C.[33] In the potential range of 0.4–0.5 V for the electric double layer charging and discharging, PtNi NW/mesoC shows higher current densities than PtNi NW/C, which is due to the difference in the BET specific surface areas of the carbon support. Electrochemically active surface areas (ECSAs) were determined based on CO stripping voaltammograms (**Table S1**) and confirmed higher $ECSA_{CO}$ for PtNi NW/mesoC than for PtNi NW/C, indicating the high catalyst dispersion on mesoC. The disappearance of anodic waves for the Pt oxide and/or hydroxide formation at >0.7 V vs. RHE for PtNi NW/mesoC indicates the suppression of surface Pt-O(H) formation for PtNi NW/mesoC (**Fig. S3a**). This could be related to the insertion of NWs into carbon mesopores.

To understand the support effects on the ORR electrocatalytic activity, linear sweep voltammograms (LSVs) of PtNi NW/mesoC and PtNi NW/C were recorded under oxygen (**Fig. 2**). Negative currents with an onset potential about 0.95 V vs. RHE indicate that the ORR occurs. Tafel slopes were determined to be about 60 mV $(dec)^{-1}$ for PtNi NW/mesoC and PtNi NW/C, indicating no obvious change in the reaction mechanism compared with conventional Pt electrodes[34] (**Fig. S4** and **Table S2**). The MAs at 0.9 V vs. RHE were determined to be 0.40 A $(mg_{Pt})^{-1}$ for PtNi NW/mesoC and 0.32 A $(mg_{Pt})^{-1}$ for PtNi NW/C, where the weight ratio of ionomer/carbon is 0.5 (I/C = 0.5) and the weight ratio of ionic liquid/carbon is zero (IL/C = 0). PtNi NW/mesoC showed higher mass activity for the ORR than PtNi NW/C and commercial Pt/C (0.14 A $(mg_{Pt})^{-1}$, **Fig. S5**). Note that PtNi NW/mesoC is more sensitive to the ionomer content than PtNi NW/C: the higher I/C ratios tended to give lower MAs for PtNi NW/mesoC whereas there is almost no effect for PtNi NW/C (**Table S1**). These results can be explained by the suppression of the mass transport of protons and/or oxygen molecules to NWs inside mesopores because ionomers such as Nafion can be placed on the surface of the support but not inside the mesopores.[1,3,18,20]

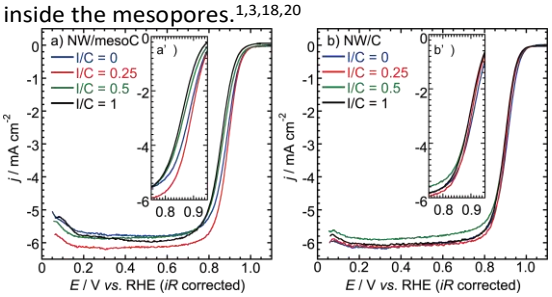

Fig. 2 LSVs of (a) PtNi NW/mesoC and (b) PtNi NW/C for different I/C ratios with a sweep rate of 10 mV s^{-1} in a 0.1 M $HClO_4$ aqueous solution under O_2 at 1600 rpm (IL/C=0). The insets show the enlarged LSVs in the range of 0.75–0.95 V vs. RHE.

The difference in the I/C sensitivity encouraged us to use the SCILL approach to PtNi NW/mesoC. For the modification of the electrocatalysts with the IL, PtNi NWs were mixed with carbon supports and [BMIM][PF_6] in the 1:1 ethanol-cyclohexane mixture under ultrasonication, and then the products were dried under vacuum (See the **SI**). Another IL of 7-methyl-1,5,7-triazabicyclo[4.4.0]dec-5-ene bis(trifluoromethane)sulfonimide, [MTBD][NTF_2], was also used for comparison. Because [BMIM][PF_6] showed a more positive effect on the ORR activity of PtNi NW/mesoC than [MTBD][NTF_2] (**Tables S3**),[11,12,14] [BMIM][PF_6] was used for further experiments. [BMIM][PF_6]-modified PtNi NW/mesoC and PtNi NW/C are hereafter referred to as IL/PtNi NW/mesoC and IL/PtNi NW/C, respectively.

IL/PtNi NW/mesoC and IL/PtNi NW/C show higher ORR activity than the corresponding unmodified ones. LSVs under oxygen enable us to determine MAs at 0.9 V vs. RHE to be 0.56 and 0.53 A $(mg_{Pt})^{-1}$ for IL/PtNi NW/mesoC and IL/PtNi NW/C with I/C = 0.5 and IL/C = 1, respectively (**Fig. 3** and **Table S4**). These values are 1.4–1.6 times higher than those in the absence of the IL. The MAs of IL/PtNi NW/mesoC increase with increasing I/C ratios: MAs of IL/PtNi NW/mesoC maximized at IL/C = 1 and I/C = 2, reaching 0.87 A $(mg_{Pt})^{-1}$ (**Table S4**). This MA is higher than those of carbon-supported PtNi nanostructured catalysts such as PtNi nanowires[28,30] or PtNi nanoframes.[35] In contrast, IL/PtNi NW/C did not follow the same trend: MAs of IL/PtNi NW/C decreased to 0.23 A $(mg_{Pt})^{-1}$ with IL/C = 1 and I/C = 1 (**Table S4**). MAs of IL/Pt/C also decreased with increasing I/C

ratios (**Fig. S6** and **Table S4**). These different trends are related to the competitive adsorption of the ionomer and IL to the catalyst. The internal environment in the carbon mesopore could suppress the ionomer poisoning for PtNi NW/mesoC even at high I/C ratios. Note that the Pt metallic state remains after the electrochemical measurements for PtNi NW/mesoC even in the presence of IL, confirmed by X-ray photoelectron spectroscopy (**Fig. S7 and Table S5**).[11,12]

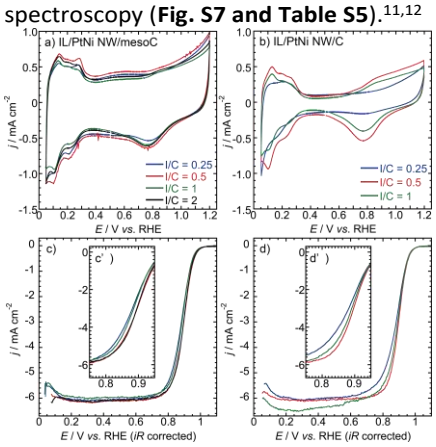

Fig. 3 CVs of (a) IL/PtNi NW/mesoC and (b) IL/PtNi NW/C with different I/C ratios recorded at 50 mV s^{-1} in a 0.1 M $HClO_4$ aqueous solution under Ar (IL/C = 1). LSVs of (c) IL/PtNi NW/mesoC and (d) IL/PtNi NW/C with different I/C ratios recorded at 10 mV s−1 and 1600 rpm in a 0.1 M $HClO_4$ aqueous solution under O2 (IL/C=1). The insets (c') and (d') show the enlarged LSVs. [BMIM][PF6] was used as the IL.

Potential-dependent SEIRA spectra of IL/PtNi NW/mesoC showed the presence of IL under electrochemical conditions (**Fig. S8**). The SEIRA spectroscopy is a surface sensitive technique and allows us to obtain vibrational information of chemical species adsorbed on the surface of electrocatalysts.[36-38] The differential SEIRA spectra of IL/NW/mesoC show negative vibrational bands at about 2960, 2935 and 2875 cm^{-1} and positive bands at about 2925, 2910 and 2855 cm^{-1}, where the spectra at 1.0 V vs. RHE were used as the references (**Fig. S8a**). The negative and positive bands are assigned to the vibrational modes of the CH_3 and CH_2 groups of $[BMIM]^+$ cations, respectively.[39] In contrast, such characteristic bands were not observed for NW/mesoC in the absence of the IL (**Fig. S8b**). These results indicate that $[BMIM]^+$ cations are present even under electrochemical conditions and the alkyl chains of $[BMIM]^+$ cations are more horizontal to the surface at more negative potentials.

Potential-dependent SEIRA spectroscopy was also performed for CO-adsorbed IL/PtNi NW/mesoC (**Fig. 4**). CO is strongly adsorbed on the Pt surface and therefore widely used as a vibrational probe molecule for SEIRA spectroscopy.[36-38] It was expected that the IL and CO could interact on the surface of PtNi NWs. At 0 V vs. RHE, a C–O stretching band centered at about 2008 cm^{-1} was observed for PtNi NW/mesoC in the absence of the IL (**Fig. 4c**). This band is assigned to the linearly bonded CO (CO_L). The peak-top wavenumber of CO_L was blue-shifted as more positive potentials were applied due to the balance between the 5σ-donation and 2π*-backdonation.[40] In the presence of the IL, a CO_L band was also observed at 0 V vs. RHE and its peak-top wavenumber depends on the applied potential.

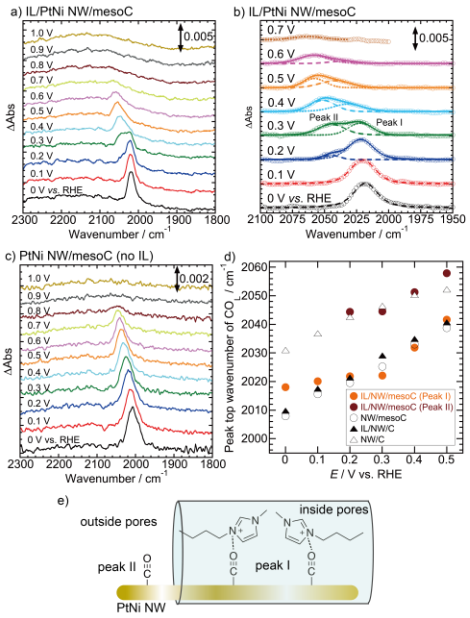

Fig. 4 Potential dependence of differential SEIRA spectra of CO-adsorbed IL/PtNi NW/mesoC (a,b) (IL/C=1, I/C=1) and (c) PtNi NW/mesoC without the IL of $[BMIM][PF_6]$ (IL/C=0, I/C=1). The potentials were changed from 0 to 1 V vs. RHE. The spectra of the catalysts with no CO-modification at the corresponding potential were used as reference spectra. Panel (b) shows enlarged spectra with deconvoluted peaks I and II for IL/PtNi NW/mesoC. The open circles indicate the experimental data. The broken or dotted lines show the fitted data using Voigt function. (d) Plots of peak-top wavenumbers of CO_L against applied potential of IL/PtNi NW/mesoC (the filled circles in orange for peak I and in wine red for peak II), PtNi NW/mesoC (the open circles), IL/PtNi NW/C (the filled triangles) and PtNi NW/C (the open triangles). (e) Sketch of the origin of peaks I and II for CO-adsorbed IL/PtNi NW/mesoC.

Two CO_L bands ranging from 0.2 to 0.6 V vs. RHE were observed for CO-adsorbed IL/PtNi NW/mesoC (**Fig. 4a** and **4b**), whereas no such band splitting was observed for CO-adsorbed IL/PtNi NW/C (**Fig. 4c**), PtNi NW/C, IL/Pt/C or Pt/C (**Fig. S9**). Thus, this band splitting is associated with the interaction of CO molecules adsorbed on the surface Pt with the IL and the mesopore. It is highly likely that $[BMIM]^+$ can interact with CO on the Pt surface because cations in electrolyte solutions can be adsorbed on the Pt surface and affect the ORR activity.[41] The two bands obtained in the peak deconvolution analysis are designated as peak I and peak II at the lower and higher wavenumbers, respectively (**Fig. 4b**).

The wavenumbers of peaks I and II for IL/PtNi NW/mesoC were plotted as a function of potential with those of peaks of CO_L for PtNi NW/mesoC, IL/PtNi NW/C and PtNi NW/C (**Fig. 4d**). Peak I shows the similar trend to PtNi NW/C, which has no mesopore or IL, while peak II shows the similar trend to PtNi NW/mesoC and IL/PtNi NW/C. Thus, peak-top wavenumbers of CO_L are red-shifted in the presence of mesopores or the IL. In other words, CO molecules interact with the internal wall of mesopores or IL, giving the lower wavenumbers as peak I (**Fig. 4e**). In contrast, no interaction of CO_L with mesopores or IL gives peak II, like PtNi NW/C. Possibly, peak II is associated with CO_L on PtNi NWs outside mesopores becoming in an IL-free environment. Such an environment can be produced by changes in the Pt surface charge because the potential showing the CO_L band splitting at 0.2 V vs. RHE is close to the potential

of zero charge for Pt(111) in a 0.1 M $HClO_4$ aqueous solution (0.3 V vs. SHE)[42] and in an IL with 0.5 M H_2O (0.1 V vs. SHE).[43] Note that almost no potential dependence of peak-top wavenumbers of CO_L at <0.2 V vs. RHE was only observed for IL/PtNi NW/mesoC (**Fig. 4d**). This is possibly due to the unique microscopic environment created by the co-presence of the IL, carbon mesopores and PtNi NWs.

Conclusions

We have demonstrated positive effects of the presence of IL on the ORR activity of PtNi NW/mesoC in acidic media. NWs are located inside mesopores, confirmed by the 3D electron transmission tomography. IL/PtNi NW/mesoC shows >1.5 times higher ORR activity than the unmodified catalyst. Potential dependent SEIRA spectra of CO-adsorbed IL/PtNi NW/mesoC have revealed the unique microscopic environment created by the IL and carbon mesopores, which is related to the activity enhancement for the ORR. Our study shows that ILs are accessible to nanospaces of less than 10 nm between NWs and carbon mesopores, providing highly reactive environments for the ORR. Our work on the SCILL approach will encourage researchers to explore nanoscale engineering of reaction space for the development of highly active electrocatalysts using not only NWs but also other nanostructured electrocatalysts.

Author contributions

M.K. and I.Y. conceived the concept. Y.K. synthesized the catalysts and Y.Z. and I.Y. optimized the synthetic conditions. Y.K. performed the electrocatalytic measurements and Y.K., S.S. and K.S. performed spectroscopic measurements. J.S., T.K. and K.S. performed 3D TEM tomography. M.K. and Y.K. took the lead in writing the manuscript. All authors discussed the results and provided suggestions for manuscript.

Conflicts of interest

There are no conflicts to declare.

Acknowledgements

The authors thank Shingo Mukai and Yusuke Kawamura (Institute for Catalysis, Hokkaido University) for their technical support on electrochemical setups and Ryo Ota (Graduate School of Engineering, Hokkaido University) and Nobumasa Yoneta (Mitsui Mining and Smelting) for taking and analyzing the three-dimensional HAADF-STEM tomography data. This work was supported by "Nanotechnology Platform" (JPMXP09A17HK0073, JPMXP09A18HK0063, JPMXP09A19HK0030 and JPMXP09A21HK0062) and “Advanced Research Infrastructure for Materials and Nanotechnology (ARIM)” (JPMXP1222HK0033, JPMXP1223HK0012 and JPMXP1224HK0036) programs of MEXT for Hokkaido University, and NEDO (JPNP20003).

Data availability

The data supporting this article have been included as part of the ESI.

References

1. K. Kodama, T. Nagai, A. Kuwaki, R. Jinnouchi and Y. Morimoto, *Nat. Nanotechnol.*, 2021, **16**, 140-147.
2. Z. Zhao, C. Chen, Z. Liu, J. Huang, M. Wu, H. Liu, Y. Li and Y. Huang, *Adv. Mater.*, 2019, **31**, 1808115.
3. L. Fan, H. Deng, Y. Zhang, Q. Du, D. Y. C. Leung, Y. Wang and K. Jiao, *Energy Environ. Sci.*, 2023, **16**, 1466-1479.
4. Y. Qiao, M. Peng, J. Lan, K. Jiang, D. Chen and Y. Tan, *J. Mater. Chem. A*, 2023, **11**, 495-511.
5. M. Chatenet, B. G. Pollet, D. R. Dekel, F. Dionigi, J. Deseure, P. Millet, R. D. Braatz, M. Z. Bazant, M. Eikerling, I. Staffell, P. Balcombe, Y. Shao-Horn and H. Schäfer, *Chem. Soc. Rev.*, 2022, **51**, 4583-4762.
6. V. R. Stamenkovic, D. Strmcnik, P. P. Lopes and N. M. Markovic, *Nat. Mater.*, 2017, **16**, 57-69.
7. M. Li, Z. Zhao, T. Cheng, A. Fortunelli, C.-Y. Chen, R. Yu, Q. Zhang, L. Gu, B. V. Merinov, Z. Lin, E. Zhu, T. Yu, Q. Jia, J. Guo, L. Zhang, W. A. Goddard, Y. Huang and X. Duan, *Science*, 2016, **354**, 1414-1419.
8. L. Chong, J. Wen, J. Kubal, F. G. Sen, J. Zou, J. Greeley, M. Chan, H. Barkholtz, W. Ding and D.-J. Liu, *Science*, 2018, **362**, 1276-1281.
9. J. Snyder, T. Fujita, M. W. Chen and J. Erlebacher, *Nat. Mater.*, 2010, **9**, 904-907.
10. J. Snyder, K. Livi and J. Erlebacher, *Adv. Funct. Mater.*, 2013, **23**, 5494-5501.
11. G.-R. Zhang, M. Munoz and B. J. M. Etzold, *Angew. Chem. Int. Ed.*, 2016, **55**, 2257-2261.
12. M. George, G.-R. Zhang, N. Schmitt, K. Brunnengräber, D. J. S. Sandbeck, K. J. J. Mayrhofer, S. Cherevko and B. J. M. Etzold, *ACS Catal.*, 2019, **9**, 8682-8692.
13. G.-R. Zhang, M. Munoz and B. J. M. Etzold, *ACS Appl. Mater. Interf.*, 2015, **7**, 3562-3570.
14. G.-R. Zhang, T. Wolker, D. J. S. Sandbeck, M. Munoz, K. J. J. Mayrhofer, S. Cherevko and B. J. M. Etzold, *ACS Catal.*, 2018, **8**, 8244-8254.
15. C. Chen, Y. J. Kang, Z. Y. Huo, Z. W. Zhu, W. Y. Huang, H. L. L. Xin, J. D. Snyder, D. G. Li, J. A. Herron, M. Mavrikakis, M. F. Chi, K. L. More, Y. D. Li, N. M. Markovic, G. A. Somorjai, P. D. Yang and V. R. Stamenkovic, *Science*, 2014, **343**, 1339-1343.
16. J. Yan and F. Mangolini, *RSC Adv.*, 2021, **11**, 36273-36288.
17. A. Hayashi, H. Notsu, K. i. Kimijima, J. Miyamoto and I. Yagi, *Electrochim. Acta*, 2008, **53**, 6117-6125.
18. V. Yarlagadda, M. K. Carpenter, T. E. Moylan, R. S. Kukreja, R. Koestner, W. Gu, L. Thompson and A. Kongkanand, *ACS Energy Lett.*, 2018, **3**, 618-621.
19. S. Ott, A. Orfanidi, H. Schmies, B. Anke, H. N. Nong, J. Hübner, U. Gernert, M. Gliech, M. Lerch and P. Strasser, *Nat. Mater.*, 2020, **19**, 77-85.
20. J. Liu and I. V. Zenyuk, *Curr. Opin. Electrochem.*, 2018, **12**, 202-208.
21. K. Chan and M. Eikerling, *J. Electrochem. Soc.*, 2011, **158**, B18.
22. L. Bu, S. Guo, X. Zhang, X. Shen, D. Su, G. Lu, X. Zhu, J. Yao, J. Guo and X. Huang, *Nat. Commun.*, 2016, **7**, 11850.

23. K. Jiang, D. Zhao, S. Guo, X. Zhang, X. Zhu, J. Guo, G. Lu and X. Huang, *Sci. Adv.*, 2017, **3**, e1601705.
24. Y. Sun, M. Luo, Y. Qin, S. Zhu, Y. Li, N. Xu, X. Meng, Q. Ren, L. Wang and S. Guo, *ACS Appl. Mater. Interf.*, 2017, **9**, 34715-34721.
25. H. Huang, K. Li, Z. Chen, L. Luo, Y. Gu, D. Zhang, C. Ma, R. Si, J. Yang, Z. Peng and J. Zeng, *J. Am. Chem. Soc.*, 2017, **139**, 8152-8159.
26. F. Kong, M. Norouzi Banis, L. Du, L. Zhang, L. Zhang, J. Li, K. Doyle-Davis, J. Liang, Q. Liu, X. Yang, R. Li, C. Du, G. Yin and X. Sun, *J. Mater. Chem. A*, 2019, **7**, 24830-24836.
27. M. Gong, Z. Deng, D. Xiao, L. Han, T. Zhao, Y. Lu, T. Shen, X. Liu, R. Lin, T. Huang, G. Zhou, H. Xin and D. Wang, *ACS Catal.*, 2019, **9**, 4488-4494.
28. M. Kato, Y. Iguchi, T. Li, Y. Kato, Y. Zhuang, K. Higashi, T. Uruga, T. Saida, K. Miyabayashi and I. Yagi, *ACS Catal.*, 2022, **12**, 259-264.
29. L. Sahoo, R. Garg, K. Kaur, C. P. Vinod and U. K. Gautam, *Nano Letters*, 2022, **22**, 246-254.
30. Y. Zhuang, Y. Iguchi, T. Li, M. Kato, Y. A. Hutapea, A. Hayashi, T. Watanabe and I. Yagi, *ACS Catal.*, 2024, **14**, 1750-1758.
31. X. Zhang, X. Dai, L. Gao, D. Xu, H. Wan, Y. Wang and L.-T. Yan, *Chem. Soc. Rev.*, 2023, **52**, 6806-6837.
32. V. R. Stamenkovic, B. Fowler, B. S. Mun, G. F. Wang, P. N. Ross, C. A. Lucas and N. M. Markovic, *Science*, 2007, **315**, 493-497.
33. M. T. Y. Paul and B. D. Gates, *Sci. Rep.*, 2019, **9**, 4161.
34. T. Shinagawa, A. T. Garcia-Esparza and K. Takanabe, *Sci. Rep.*, 2015, **5**, 13801.
35. M. Kato, R. Nakahoshiba, K. Ogura, S. Tokuda, S. Yasuda, K. Higashi, T. Uruga, Y. Uemura and I. Yagi, *ACS Appl. Energy Mater.*, 2020, **3**, 6768-6774.
36. M. Kato, K. Ogura, S. Nakagawa, S. Tokuda, K. Takahashi, T. Nakamura and I. Yagi, *ACS Omega*, 2018, **3**, 9052-9059.
37. P. Li, Y. Jiang, Y. Hu, Y. Men, Y. Liu, W. Cai and S. Chen, *Nat. Catal.*, 2022, **5**, 900-911.
38. K. Zhao, X. Chang, H.-S. Su, Y. Nie, Q. Lu and B. Xu, *Angew. Chem. Int. Ed.*, 2022, **61**, e202207197.
39. L. J. Richter, T. P. Petralli-Mallow and J. C. Stephenson, *Optics Letters*, 1998, **23**, 1594-1596.
40. D. K. Lambert, *Electrochim. Acta*, 1996, **41**, 623-630.
41. T. Kumeda, H. Tajiri, O. Sakata, N. Hoshi and M. Nakamura, *Nat. Commun.*, 2018, **9**, 4378.
42. K. Ojha, N. Arulmozhi, D. Aranzales and M. T. M. Koper, *Angew. Chem. Int. Ed.*, 2020, **59**, 711-715.
43. A. Kemna and B. Braunschweig, *J. Phys. Chem. Lett.*, 2020, **11**, 7116-7121.